Open access • Journal Article • DOI:10.1038/S41589-018-0145-X

Structural insights into binding specificity, efficacy and bias of a beta2AR partial agonist. — Source link

Matthieu Masureel, Yaozhong Zou, Louis Picard, Emma T van der Westhuizen ...+13 more authors

Institutions: Stanford University, Université de Montréal, Monash University, D. E. Shaw Research ...+4 more institutions

Published on: 16 Oct 2018 - Nature Chemical Biology (Nature Publishing Group)

Topics: Agonist, Partial agonist and Salmeterol

Structural insights into binding specificity, efficacy and bias of a β2AR partial agonist.

Masureel, Matthieu; Zou, Yaozhong; Picard, Louis-Philippe; van der Westhuizen, Emma; Mahoney, Jacob P; Rodrigues, João P G L M; Mildorf, Thomas J; Dror, Ron O; Shaw, David E; Bouvier, Michel; Pardon, Els; Steyaert, Jan; Sunahara, Roger K; Weis, William I; Zhang, Cheng; Kobilka, Brian K

Published in:
Nature Chemical Biology

DOI:
10.1038/s41589-018-0145-x

Publication date:
2018

nature chemical biology

ARTICLES

https://doi.org/10.1038/s41589-018-0145-x

Structural insights into binding specificity, efficacy and bias of a β_2AR partial agonist

Matthieu Masureel[1,17], Yaozhong Zou[1,2,17], Louis-Philippe Picard[3], Emma van der Westhuizen[3,13], Jacob P. Mahoney[4,14], João P. G. L. M. Rodrigues[1,5,6], Thomas J. Mildorf[7,15], Ron O. Dror[7,16], David E. Shaw[7,8], Michel Bouvier[3], Els Pardon[9,10], Jan Steyaert[9,10], Roger K. Sunahara[11], William I. Weis[1,6], Cheng Zhang[12*] and Brian K. Kobilka[1*]

Salmeterol is a partial agonist for the β_2 adrenergic receptor (β_2AR) and the first long-acting β_2AR agonist to be widely used clinically for the treatment of asthma and chronic obstructive pulmonary disease. Salmeterol's safety and mechanism of action have both been controversial. To understand its unusual pharmacological action and partial agonism, we obtained the crystal structure of salmeterol-bound β_2AR in complex with an active-state-stabilizing nanobody. The structure reveals the location of the salmeterol exosite, where sequence differences between β_1AR and β_2AR explain the high receptor-subtype selectivity. A structural comparison with the β_2AR bound to the full agonist epinephrine reveals differences in the hydrogen-bond network involving residues Ser204$^{5.43}$ and Asn293$^{6.55}$. Mutagenesis and biophysical studies suggested that these interactions lead to a distinct active-state conformation that is responsible for the partial efficacy of G-protein activation and the limited β-arrestin recruitment for salmeterol.

G-protein-coupled receptors (GPCRs) are able to respond to a large variety of ligands with different efficacy profiles for specific signaling pathways[1]: full agonists that maximally stimulate; partial agonists that produce submaximal stimulation even at fully saturating concentrations; inverse agonists that suppress basal signaling; and neutral antagonists that bind the receptor without stimulating or inhibiting basal signaling. Among these categories, partial agonists are often better tolerated than full agonists as therapeutics[2].

Salmeterol is a partial agonist for the human β_2AR. As a potent bronchodilator, it is among the most prescribed drugs for the treatment of asthma and chronic obstructive pulmonary disease (COPD)[3]. Compared with some other β_2AR agonists such as isoproterenol and salbutamol, salmeterol has two desirable pharmacological properties. First, salmeterol is able to distinguish β_2AR from β_1AR for selective stimulation (1,400- to 3,000-fold selectivity)[4], thereby minimizing cardiac toxicity[5]. Second, salmeterol belongs to the class of long-acting β_2AR agonists (LABAs), which have a duration of action up to 12 h, in contrast to the short-acting β_2AR agonists, such as salbutamol, which have only a 4- to 6-h duration of action[6–8]. Those pharmacological properties of salmeterol have contributed to its successful use in treating asthma and COPD for more than two decades. However, LABAs, especially salmeterol, when used alone, have been suggested to be associated with increased mortality in asthmatics in several clinical trials. This liability is mitigated when LABAs are combined with an inhaled corticosteroid[9–11].

The high selectivity and long-acting properties of salmeterol have been attributed to its unusual bitopic structure. In addition to the saligenin ethanolamine pharmacophore that replaces the catecholamine structure of the endogenous β_2AR ligand epinephrine (also known as adrenaline), salmeterol contains an additional moiety of an aryloxyalkyl tail consisting of a phenol ring with an 11-atom ether chain (Fig. 1a). While the pharmacophore binds the orthosteric site, which is responsible for receptor activation, the aryloxyalkyl tail has been proposed to bind to an additional site (exosite), thus allowing for additional interactions responsible for the high receptor-subtype selectivity and the slow dissociation rate contributing to its long duration of action[12]. Previous mutagenesis and biochemical studies seeking to locate the exosite have yielded conflicting results[4,12–16]. Salmeterol is also of interest because it is a functionally selective β_2AR partial agonist with a 5- to 20-fold bias toward Gs over arrestin[17,18]. Previous studies have revealed that activation of the β_2AR by salmeterol, compared with isoproterenol, leads to slower initial rates of G-protein-coupled receptor kinase (GRK) phosphorylation and similar maximal degrees of phosphorylation[19,20], but strongly decreased arrestin-mediated receptor internalization and desensitization[17,21,22], thus contributing to the prolonged therapeutic effect of salmeterol in bronchial dilation as a result of β_2AR stimulation. This

[1]Department of Molecular and Cellular Physiology, Stanford University School of Medicine, Stanford, CA, USA. [2]Geneus Technologies, Ltd, Chengdu, Sichuan, People's Republic of China. [3]Department of Biochemistry, Institute for Research in Immunology and Cancer, Université de Montreal, Montreal, Québec, Canada. [4]Department of Pharmacology, University of Michigan, Ann Arbor, MI, USA. [5]Department of Computer Science, Stanford University, Stanford, CA, USA. [6]Department of Structural Biology, Stanford University, Stanford, CA, USA. [7]D. E. Shaw Research, New York, NY, USA. [8]Department of Biochemistry and Molecular Biophysics, Columbia University, New York, NY, USA. [9]Structural Biology Brussels, Vrije Universiteit Brussel, Brussels, Belgium. [10]Structural Biology Research Center, VIB, Brussels, Belgium. [11]Department of Pharmacology, University of California San Diego School of Medicine, La Jolla, CA, USA. [12]Department of Pharmacology and Chemical Biology, University of Pittsburgh School of Medicine, Pittsburgh, PA, USA. [13]Present address: Monash Institute for Pharmaceutical Sciences, Monash University, Victoria, Australia. [14]Present address: Department of Molecular and Cellular Physiology, Stanford University School of Medicine, Stanford, CA, USA. [15]Present address: Dropbox, New York, NY, USA. [16]Present address: Department of Computer Science and Institute for Computational and Mathematical Engineering, Stanford University, Stanford, CA, USA. [17]These authors contributed equally: Matthieu Masureel, Yaozhong Zou. *e-mail: chengzh@pitt.edu; kobilka@stanford.edu

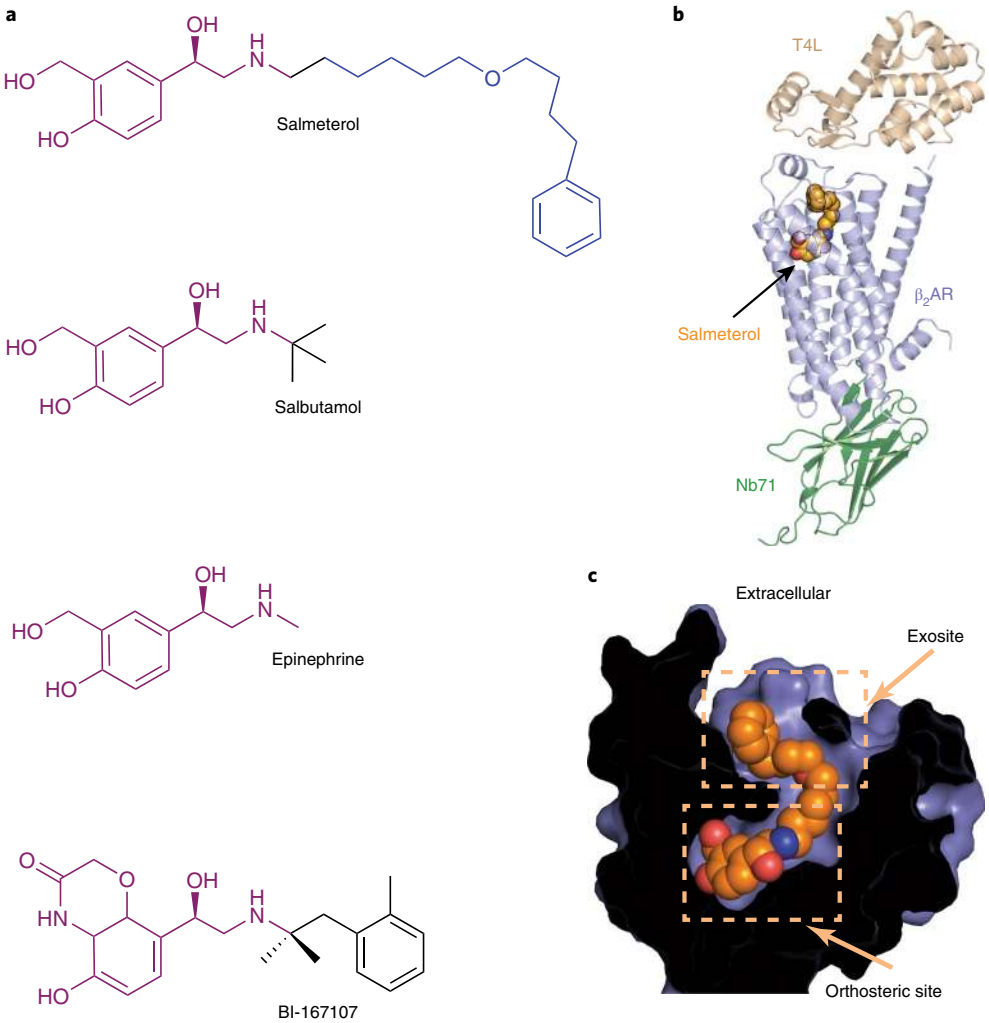

Fig. 1 | Crystal structure of salmeterol-bound β_2AR. a, Chemical structures of the following β_2AR ligands: partial agonists salmeterol and salbutamol; full agonists epinephrine and BI-16707. The respective pharmacophores that bind the orthosteric ligand-binding pocket are highlighted in purple, and the aryloxyalkyl tail of salmeterol, which binds the exosite, is highlighted in blue. **b**, Overall ribbon representation of the salmeterol-bound β_2AR–Nb71 complex. The T4L lysozyme fusion facilitates crystallization, and Nb71 stabilizes the active, salmeterol-bound (orange spheres) β_2AR. **c**, Cross-section through the receptor, with the interior in black, highlighting salmeterol (orange spheres) occupying the orthosteric site and the exosite.

signaling bias may contribute to the advantageous therapeutic profile of salmeterol by maintaining bronchodilation through Gs-mediated signaling while minimizing arrestin-mediated β_2AR desensitization and avoiding arrestin-dependent proinflammatory effects[23,24].

Recent progress in the structural characterization of β adrenergic receptors, especially the crystal structures of active β_2AR bound to the full agonists BI-167107 or epinephrine, with either a Gs protein or active-state-stabilizing nanobody, as well as the crystal structures of inactive avian β_1AR bound to a variety of full and partial agonists, have greatly advanced understanding of the pharmacology and activation of β adrenergic receptors[25–29]. To further understand the molecular basis for the unusual pharmacological properties of salmeterol and its partial agonism, we obtained the crystal structure of salmeterol-bound human β_2AR in an active state stabilized by a conformation-specific nanobody, Nb71. The structure reveals the location of the exosite and provides a structural explanation for the high receptor-subtype selectivity and distinct signaling behavior of salmeterol.

Results

Nanobody Nb71 stabilizes salmeterol-bound β_2AR. For the β_2AR and the μ-opioid receptor, agonists alone are insufficient to stabilize the receptors in active conformational states[27,30–32]. As a result, the active-state structures of the β_2AR and μ-opioid receptor have required either a G protein or conformation-specific camelid antibody fragments (nanobodies) to stabilize the active states of the receptors[25,26,29]. The first active-state structure of a hormone-activated GPCR was obtained with a nanobody named Nb80, which was obtained from a llama immunized with β_2AR bound to the ultra-high-affinity full agonist BI-167107 reconstituted into phospholipid vesicles[25]. The structures of β_2AR in the β_2AR–Nb80 complex and the β_2AR–Gs complex are very similar[25,26]. However, evidence from biophysical studies suggests that partial agonists may stabilize distinct states[33]; consequently, Nb80 may not be the best candidate to stabilize salmeterol-bound β_2AR.

Whereas Nb80 preferentially binds agonist-occupied β_2AR rather than antagonist-occupied β_2AR[25], Octet RED studies indicated that Nb80 also preferentially binds β_2AR bound to BI-167107 and epinephrine rather than β_2AR bound to salmeterol (Supplementary Table 1). Moreover, Nb80 has a greater effect in enhancing the binding affinity of the agonist isoproterenol than the partial agonist salmeterol (Supplementary Fig. 1). We therefore selected another nanobody, Nb71, generated from the same immunization that produced Nb80. Nb71 preferentially binds agonist-occupied β_2AR[34], but, in contrast to Nb80, it has no preference for these catecholamines

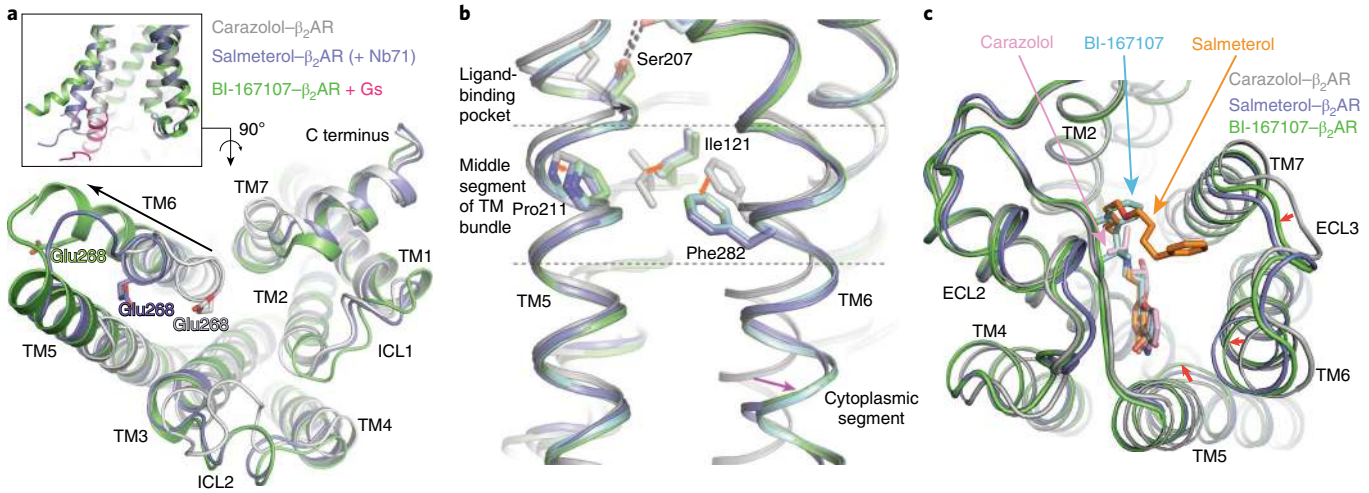

Fig. 2 | Structural features of the β_2AR–salmeterol–Nb71 complex. a–c, Overlay of inactive carazolol-bound receptor (gray), Nb71- and salmeterol-bound β_2AR (blue), and BI-167107-bound β_2AR–Gs complex (green and pink, respectively). **a**, Side view (inset) and cytoplasmic view of TM6, showing the position of TM6 relative to the helical bundle. The extent of TM6 movement, indicated by black arrows, was measured with the Cα of Glu268 as a reference point. **b**, Rearrangement of Pro211$^{5.50}$, Ile121$^{3.40}$ and Phe282$^{6.44}$ and the associated outward movement of the cytoplasmic end of TM6. The inactive structure of β_2AR is gray. The active structures of β_2AR are blue (coupled with salmeterol and Nb71), cyan (coupled with epinephrine and 6B9) and green (coupled with BI-167107 and Gs). **c**, Extracellular (top) view of β_2AR, with major conformational changes among structures indicated by red arrows and ligands shown in stick representation.

over salmeterol (Supplementary Table 1 and Supplementary Fig. 1). Therefore, we chose Nb71 to stabilize the salmeterol-bound β_2AR for structural characterization.

Structural features of Nb71-stabilized β_2AR. We used an engineered β_2AR with T4 lysozyme (T4L) fused to its N-terminal region and a truncated intracellular loop3 (referred to as T4L-β_2AR-ΔICL3 hereafter) to crystallize β_2AR bound to salmeterol. Previous studies have demonstrated that T4L-β_2AR-ΔICL3 exhibits similar ligand binding and G-protein-activating properties to those of the wild-type β_2AR[35]. Using this construct, we obtained crystals of the β_2AR–salmeterol–Nb71 complex through the lipidic cubic phase method[36]. A complete dataset was obtained by merging data from 23 crystals, and the structure was determined to a resolution of 3.0 Å (Fig. 1b,c and Supplementary Table 2). Like Nb80, Nb71 binds the cytoplasmic surface of the receptor with its third complementarity-determining-region loop inserted into a hydrophobic cavity formed by residues from transmembrane helices (TMs) 3, 5, 6 and 7 (Fig. 1b and Supplementary Fig. 2), yet Nb71 stabilizes a conformation distinct from that stabilized by Nb80 (Supplementary Fig. 2).

The active-state conformation of the receptor in the β_2AR–salmeterol–Nb71 complex resembles that of the BI-167107-bound β_2AR in complex with Nb80 (PDB 3P0G, r.m.s. deviation 1.0 Å) or with Gs (PDB 3SN6, r.m.s. deviation 1.3 Å) more than the inactive-state conformation of the receptor in the structure of β_2AR bound to the inverse agonist carazolol (PDB 2RH1, r.m.s. deviation 1.9 Å)[25,26]. Indeed, the structural features associated with receptor activation[25], including the outward movement of TM6 at the cytoplasmic side associated with the conformational changes of the core triad residues Pro211$^{5.50}$, Ile121$^{3.40}$ and Phe282$^{6.44}$ (Ballesteros–Weinstein numbering), as well as the slightly contracted ligand-binding pocket at the extracellular side, are all present in the structure of the β_2AR–salmeterol–Nb71 complex, as compared with the inactive β_2AR (Fig. 2a–c). However, the Nb71-stabilized β_2AR shows some structural features distinct from those of the Nb80- and Gs-stabilized β_2AR. Relative to the inactive β_2AR, the Nb71-stabilized β_2AR displays a smaller outward movement of the cytoplasmic end of TM6 (8 Å) than the Nb80-stabilized β_2AR (11 Å) or Gs-stabilized β_2AR (13 Å) (Fig. 2a). There is also a slightly smaller counterclockwise rotation of TM6 in the Nb71-stabilized β_2AR when viewed from the cytoplasmic surface, as shown by the position of Glu268 (Fig. 2a). Although this current structure clearly shows an active-state conformation of β_2AR, the smaller conformational rearrangements observed for TM6 after activation, as compared with the changes seen for the active-state-stabilized β_2AR bound to Nb80 or Gs, suggest a less active or a partially active conformational state of β_2AR stabilized by Nb71. This partially active conformational state might potentially closely resemble a salmeterol-stabilized conformation of β_2AR that is less efficient at coupling to Gs. However, the conformation of TM6 is primarily stabilized by interactions with Nb71 and may not reflect the conformation stabilized by salmeterol alone.

Exosite binding of salmeterol. The location and the molecular details of the exosite for the aryloxyalkyl tail of salmeterol are of great interest because of its association with the high receptor selectivity, high affinity and long-lasting action of salmeterol. The clear electron density map of salmeterol based on our structure allowed us to unambiguously define the structural basis of the exosite (Fig. 3a,b and Supplementary Figs. 3 and 4). The crystal structure shows that the aryloxyalkyl tail of salmeterol extends toward the extracellular surface of the receptor, occupying a cleft formed by residues from extracellular loop (ECL) 2, ECL3 and the extracellular ends of TM6 and TM7. Interactions between salmeterol and the exosite are mediated primarily through extensive van der Waals and hydrophobic interactions (Fig. 3c). The phenol ring of the tail also forms π–π interactions with the surrounding aromatic residues Phe194^{ECL2}, Tyr308$^{7.35}$ and His296$^{6.58}$, in agreement with previous studies reporting a 5- to 18-fold decrease in salmeterol affinity caused by mutation of those residues[4]. In addition, the ether oxygen atom of the tail forms a hydrogen bond with the main chain amide group of residue Phe193^{ECL2} (Fig. 3a). This ether oxygen atom acts as a 'hinge' point where the tail of salmeterol bends almost 90° to fit the exosite. Previous studies have indicated that shifting or removing the ether oxygen in the aryloxyalkyl tail substantially decreases the affinity of salmeterol for β_2AR[21], thus suggesting an important role of this hydrogen bond in exosite binding (Supplementary Fig. 5). All those

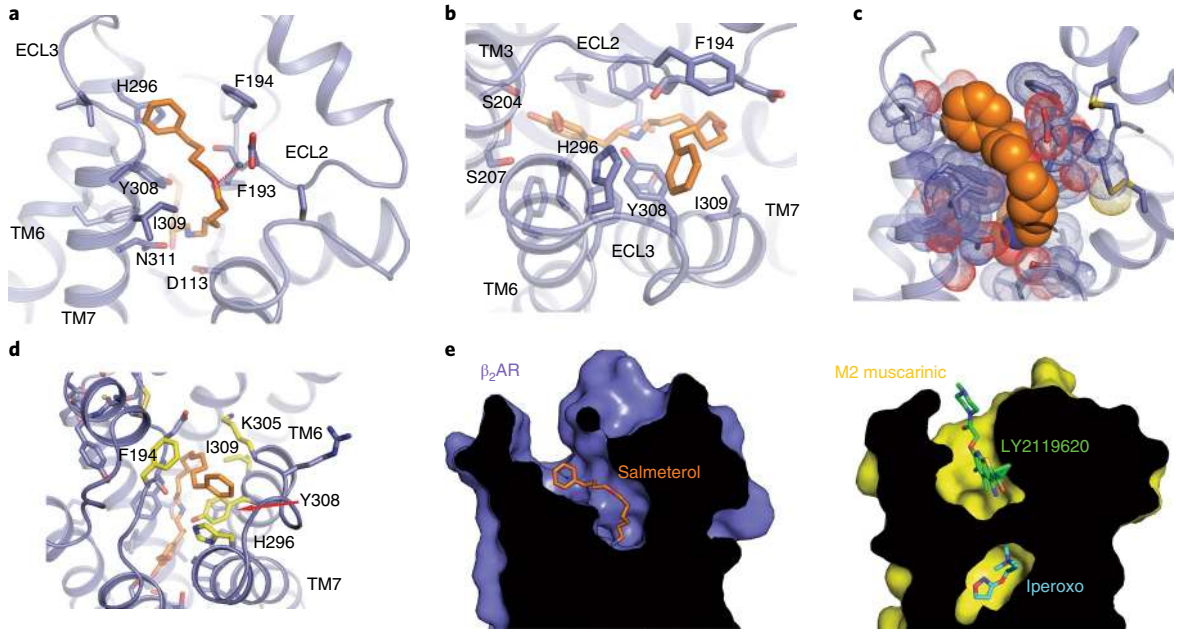

Fig. 3 | Salmeterol exosite and receptor-subtype-selectivity determinants. a,**b**, Side (**a**) and top (**b**) views of β_2AR, with stick representation of salmeterol (orange). **c**, Spherical representation of the salmeterol aryloxyalkyl moiety (orange) and the β_2AR (blue). **d**, Residues important for interaction and specificity are highlighted in yellow and labeled. With the exception of Y308 (indicated by a red arrow), the amino acids that form the orthosteric binding pocket for epinephrine are identical between β_1AR and β_2AR. **e**, Comparison of the ligand-binding sites between β_2AR (left) bound to salmeterol (orange sticks) and M2R (right) bound to the allosteric modulator LY2119620 (green sticks).

additional interactions in the exosite contribute to the 1,000-fold-higher affinity of salmeterol over salbutamol, a short-acting β_2AR agonist that shares the same orthosteric pharmacophore as salmeterol but lacks the long aryloxyalkyl tail[37] (Fig. 1a).

The exosite binding also explains the very high selectivity of salmeterol for β_2AR over β_1AR (>3,000 fold)[37]. β_1AR and β_2AR share a very high overall structural similarity (r.m.s. deviation of carazolol-bound avian β_1AR and human β_2AR = 0.58 Å; PDB 2YCW and PDB 2RH1, respectively) and sequence similarity (92% in TM segments for human β_1AR and β_2AR; Supplementary Fig. 6). In particular, all residues that form the orthosteric binding pocket, with the exception of Tyr308, are identical in β_1AR and β_2AR. In contrast, the exosite is relatively divergent in those two receptors. Salmeterol achieves high receptor selectivity by sampling this divergent region with its long aryloxyalkyl tail (Fig. 3d and Supplementary Fig. 6). Such selectivity determinants do not apply to salbutamol, which has only approximately 20-fold selectivity for β_2AR over β_1AR[37]. Our results are in agreement with extensive chimeric-receptor and site-directed-mutagenesis studies recently reported by Baker et al.[4], who have observed that the K305D and H296K mutations in the β_2AR substantially affect salmeterol affinity but have little effect on salbutamol affinity.

The salmeterol exosite in β_2AR is reminiscent of the well-defined allosteric site in the M2 muscarinic receptor (M2R)[38]. The M2R is one of the most extensively characterized model systems for allosteric regulation. We compared the exosite in the β_2AR and the binding site for the positive allosteric modulator LY2119620 (Fig. 3e), as revealed by the active-state crystal structure of M2R bound to the orthosteric agonist iperoxo and LY2119620 (ref. [38]). The similarity between those two sites suggests the potential for allosteric regulation of β_2AR activity by small molecules that target the exosite. However, the bitopic nature of salmeterol with two-site binding on β_2AR supports the feasibility of developing highly selective bitopic compounds for other GPCRs including muscarinic receptors[39].

Polar interactions within the orthosteric binding site. Although the interactions between the aryloxyalkyl tail of salmeterol and the exosite in the extracellular vestibule of β_2AR confer the high affinity and selectivity of salmeterol, they are not responsible for its efficacy and signaling bias. Salmeterol and salbutamol exhibit similar signaling properties including partial agonism and the selective activation of Gs over arrestin and Gi[17] (Supplementary Fig. 7), despite their differences in affinity and receptor selectivity. Given that salmeterol and salbutamol share only the saligenin ethanolamine pharmacophore (Fig. 1a), the interactions between this shared pharmacophore and the receptor within the orthosteric binding pocket are likely to be responsible for their shared signaling properties. In the orthosteric binding site, the alkylamine and β-hydroxyl groups of salmeterol form hydrogen-bonding interactions with Asp113$^{3.32}$ and Asn312$^{7.39}$, and the saligenin group forms hydrogen-bonding interactions with Ser203$^{5.42}$ and Ser207$^{5.46}$, which are similar to the interactions observed for β_2AR bound to the full agonist epinephrine (Fig. 4a,b). In the structure of β_2AR bound to epinephrine, the hydrogen-bonding interactions with Ser203$^{5.42}$ and Ser207$^{5.46}$ are associated with the inward movement of TM5 around those two serine residues, which is further linked to the rearrangement of the core triad residues and the outward movement of the cytoplasmic end of TM6 (ref. [29]). For salmeterol, the two saligenin hydroxyl groups also form direct hydrogen-bonding interactions with Ser203$^{5.42}$ and Ser207$^{5.46}$. However, these interactions with salmeterol, compared with those with epinephrine, may have a weaker effect on stabilizing the inward movement of TM5 because of the additional methylene between the *meta*-position hydroxyl group and the phenyl ring.

In epinephrine-bound β_2AR, Asn293$^{6.55}$ forms a hydrogen bond with Ser204$^{5.43}$ and the *meta*-hydroxyl of epinephrine. This polar network is not observed in the salmeterol-bound β_2AR. Asn293$^{6.55}$ and Ser204$^{5.43}$ have previously been shown to be important for the binding of epinephrine but not for the binding of antagonists[40,41]. To further investigate the possible role of these polar networks in ligand efficacy, we used molecular dynamics (MD) simulations to characterize the stability of specific ligand–receptor hydrogen bonds that would be expected to stabilize the inward movement of TM5 and

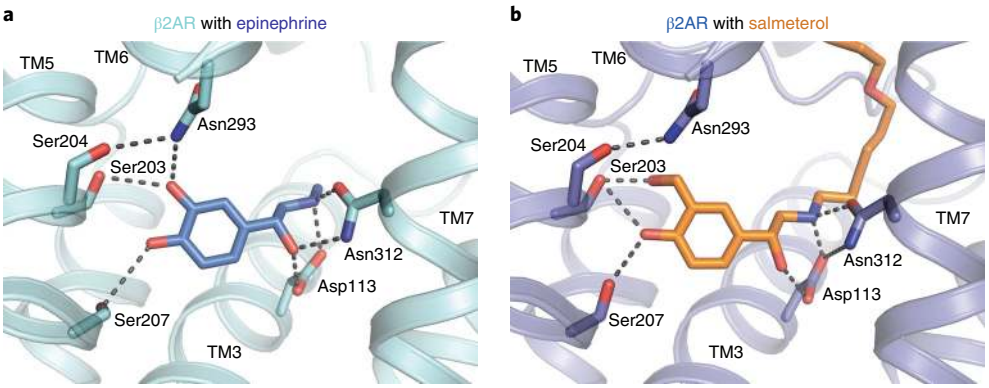

Fig. 4 | Hydrogen-bonding interactions in the orthosteric site and rearrangement of the ligand-binding pocket. a,**b**, Comparison of ligand-mediated hydrogen bonds (black dashed lines) in epinephrine-bound (**a**) and salmeterol-bound (**b**) β_2AR.

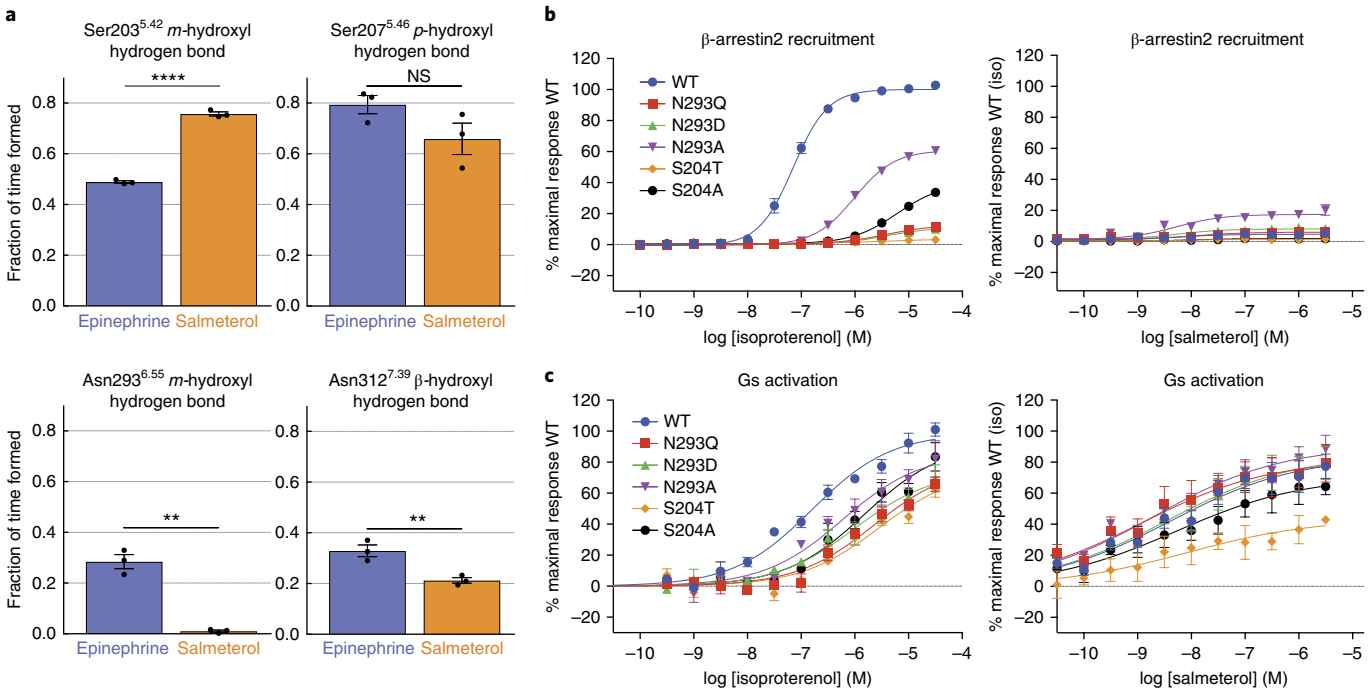

Fig. 5 | Ligands and specific residues in the orthosteric site modulate hydrogen-bonding and signaling outcome. a, Frequency of hydrogen-bonding between Ser203$^{5.42}$ and Asn293$^{6.55}$ and the ligand *m*-OH group; Ser207$^{5.46}$ and the ligand *p*-OH group; and Asn312$^{7.39}$ and the ligand β-OH group in MD simulations of receptor bound to epinephrine or salmeterol. Individual data points (black dots) and s.e.m. (error bars) of 3 independent experiments are shown. Statistical significance was assessed with one-sided Welch's unequal variance *t* test (*P* values: ****Ser203$^{5.42}$ = 0.00003; Ser207$^{5.46}$ = 0.08 (nonsignificant, NS); **Asn293$^{6.55}$ = 0.004; **Asn312$^{7.39}$ = 0.01). The actual statistical significance of the differences (for example, for Ser207) may be higher than computed, because each of the data points is based on a trajectory with thousands of samples. **b**,**c**, BRET-based assays monitoring β-arrestin2 recruitment (**b**) and G-protein activation (**c**) on wild-type (WT) and the indicated mutant β_2AR constructs. Data represent the mean (symbols) ± s.e.m. (error bars) of 3 independent experiments. Error bars shorter than the height of the symbol are not shown.

the rotation of TM6 observed in active-state structures of the β_2AR (Fig. 5a). These simulations show that salmeterol forms less stable hydrogen bonds with Asn293$^{6.55}$ and Asn312$^{7.39}$ than does epinephrine. Salmeterol forms a more stable hydrogen bond with Ser203$^{5.42}$, apparently only because its longer hydroxymethyl group can maintain this hydrogen bond better than epinephrine's hydroxyl group, even when TM5 moves away from its crystallographic position. Thus, although the salmeterol-bound crystal structure captured a binding-pocket conformation similar to that observed for the full agonist, MD simulations suggest that this active conformation is stabilized less by salmeterol than by epinephrine, and the most dramatic difference was observed for Asn293$^{6.55}$. To further characterize the role of Asn293$^{6.55}$ and Ser204$^{5.43}$ interactions, we examined the effects of mutating these residues on β-arrestin2 recruitment and Gs activation by using bioluminescence resonance energy transfer (BRET) between membrane-anchored GFP and luciferase-tagged arrestin or luciferase-tagged Gs and GFP-tagged $G_{\beta 1}/G_{\gamma 1}$, respectively[42,43] (Fig. 5b,c and Supplementary Table 3). For all the mutations tested in the presence of isoproterenol, a catecholamine similar to epinephrine, we observed a dramatic decrease in β-arrestin2 recruitment (Fig. 5b) and a more moderate decrease in Gs activation (Fig. 5c). This result suggests an important role of these two residues in regulating bias, either by directly modulating arrestin coupling or by altering GRK phosphorylation and hence arrestin binding.

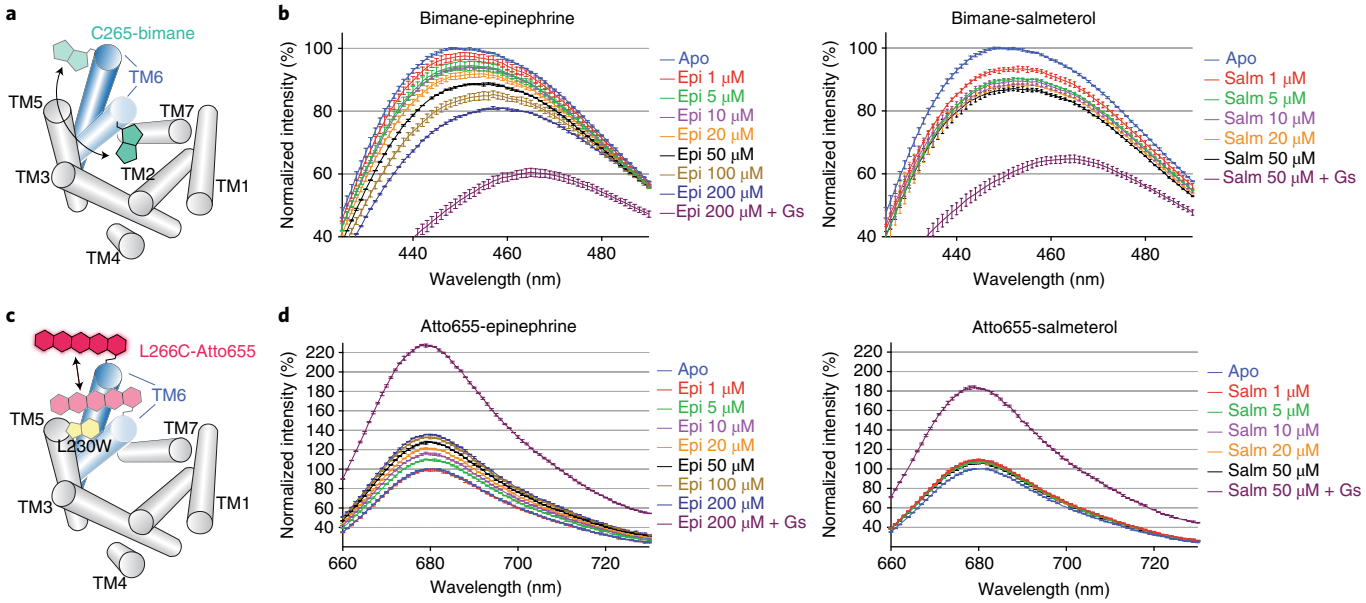

Fig. 6 | Spectroscopic interrogation of ligand-induced changes in TM6 conformation on detergent-solubilized, purified labeled receptor. a,**c**. Schematic representation of labeled receptor constructs used to probe the outward motion of TM6. The β_2AR transmembrane helices 1–5 and 7 are shown as gray cylinders. The blue cylinders represent TM6 in the inactive (light blue) and active (dark blue) conformations, with the labels attached at the intracellular end of TM6 depicted according to their overall structure. The bimane fluorophore (teal) is an environment-sensitive reporter, whereas the Atto655 dye (pink) is quenched in a distance-dependent manner by an engineered tryptophan (L230W, yellow). **b**,**d**, Steady-state fluorescence emission spectra of bimane-labeled (**b**) and Atto655-labeled (**d**) receptor in the presence of epinephrine (epi) or salmeterol (salm). The spectra are normalized relative to ligand-free receptor (apo; light-blue curve) and show the fluorescence dose–response curves of receptors up to saturating ligand concentrations, in the absence or presence of G protein. Data are plotted as mean (curves) ± s.d. (error bars) of triplicate measurements.

Interestingly, the same mutations, with the exception of S204T, had a less pronounced effect on the ability of salmeterol to activate Gs (Fig. 5c), and all mutants showed very little or no salmeterol-induced arrestin recruitment, similarly to wild-type β_2AR (Fig. 5b). Thus, the absence of the hydrogen bonds between Asn293$^{6.55}$ and salmeterol may account for the weak β-arrestin recruitment as well as the lower efficacy in Gs activation of salmeterol-bound β_2AR compared with β_2AR bound to full agonist.

Spectroscopic insights into salmeterol-bound β_2AR. The differences in efficacy and signaling bias between salmeterol and the full agonist epinephrine suggest that salmeterol may stabilize a distinct conformation. Previous single-molecule Förster resonance energy transfer (FRET) studies have suggested a smaller outward displacement of TM6 in β_2AR bound to salmeterol compared with β_2AR bound to epinephrine or BI167107 (ref. [33]). In addition, cellular assays using a BRET-based β_2AR conformational sensor[44] confirmed salmeterol's lower propensity to promote the outward movement of TM6 (Supplementary Fig. 8). Nevertheless, these FRET studies were unable to distinguish the mechanistic possibilities of whether salmeterol either stabilizes the same conformation of TM6 as epinephrine but does so for a smaller receptor population, or stabilizes a distinct TM6 conformation. To further investigate the differences at the cytoplasmic end of TM6 after activation between salmeterol-bound and epinephrine-bound β_2AR in the absence of conformation-stabilizing nanobodies, we performed steady-state spectroscopic studies on purified, labeled receptor in detergent with two different reporter systems (Supplementary Fig. 9a). We used β_2AR labeled at Cys265 with the fluorophore monobromobimane (bimane or mBBr), which we previously used as a conformational reporter of β_2AR activation[31,45], and developed a new fluorescent reporter system using an engineered β_2AR labeled at residue 266 with the fluorophore Atto655.

The bimane fluorophore has been extensively used to report on the activation of β_2AR[25,45,46] as well as other GPCRs[47,48], because it is very sensitive to its chemical environment. In the inactive state, bimane attached at the cytoplasmic end of TM6 is in a hydrophobic environment. After receptor activation, the intracellular end of TM6 undergoes an outward and 'unwinding' motion (Fig. 6a) that shifts bimane to a more polar and solvent-exposed environment, thus resulting in a decrease in fluorescence intensity and a redshift in wavelength of maximum emission intensity (λ_{max}). Agonists alone produced a 10–20% decrease in intensity and an ~10-nm redshift in λ_{max}. Further changes were observed after G-protein coupling. Using this reporter system, we found that even though salmeterol has a higher binding affinity than epinephrine to β_2AR[6], epinephrine causes a larger decrease than salmeterol in the intensity and redshift in λ_{max} of bimane when both ligands are used at saturating concentrations (Fig. 6b). This result suggests that salmeterol stabilizes β_2AR in conformations with on average a smaller outward movement or rotation of TM6. In addition, we observed that Gs induced similar bimane responses with salmeterol and epinephrine (Fig. 6b; '+Gs' curves), thus indicating that, once coupled to Gs, the β_2AR adopts a similar TM6 conformation regardless of which agonist is bound at the extracellular region, in agreement with previous single-molecule FRET studies[33]. Nevertheless, the extent to which the salmeterol-bound receptor couples to Gs appears to be slightly lower, because the change in λ_{max} and fluorescence intensity is slightly less pronounced than that for the epinephrine-bound receptor.

To complement the bimane-based measurements, we developed a new distance-sensitive fluorescent reporter. Rather than relying on FRET, in which stoichiometric and specific labeling of donor and acceptor is required to faithfully report on distance changes in bulk measurements, we used a single-dye reporter system. In photoinduced electron transfer (PET), fluorophores such as Atto655 can be quenched by a tryptophan in proximity, through the formation of weakly fluorescent or nonfluorescent dye–tryptophan ground-state complexes[49] (Fig. 6c). Owing to the strong distance dependence of PET, small-scale conformational changes result in 'on/off' switching of fluorescence, thus

yielding a change in fluorescence intensity but no shift in λ_{max} over a small distance range, typically approximately 5–10 Å (ref. [49]).

To report on only the outward motion of TM6, we chose to label Leu266 mutated to cysteine instead of the native Cys265, because the former does not undergo inward-to-outward rotations after activation but points outward in both active and inactive structures (Supplementary Fig. 9a). On the basis of the inactive and active β_2AR crystal structures and dye simulations (Supplementary Fig. 9b), we speculated that a tryptophan residue introduced at the intracellular end of TM5 (L230W) would quench the fluorescence of Atto655 in the inactive state, but the quenching would be considerably less in the active state, because the distance range and change between TM5 and TM6 that occurs after activation should be compatible with PET-induced quenching. By simulating the conformational ensembles of Atto655 bound to Cys266 in the inactive and active β_2AR structures, we found an average dye–Trp230 distance change of approximately 5 Å after receptor activation (Supplementary Fig. 9b), a result compatible with the reported quenching distance. We therefore introduced mutations L230W and L266C into a minimal-cysteine-background β_2AR[33] and verified that the detergent-purified, Atto655-labeled β_2ARΔ6 L230W L266C construct retained wild-type ligand binding properties (Supplementary Fig. 10).

When measuring the steady-state fluorescence emission of Atto655-labeled β_2ARΔ6 L230W L266C, subsequently referred to as Atto-β_2AR, in the presence of saturating concentrations of epinephrine, we observed an ~30% increase in fluorescence intensity compared with that of ligand-free receptor, findings compatible with an outward motion of TM6 and an increased distance between Atto655 and the Trp230 quencher on TM5 (Fig. 6d and Supplementary Fig. 11a). Given the short distance over which PET quenching occurs, this observation probably reflects a TM6 displacement of ~5 Å or more in ~30% of epinephrine-bound receptors. This result is consistent with the fraction of receptors in an active conformation observed in double electron–electron resonance spectroscopy studies[31]. Interestingly, we observed a much smaller difference (<10%) between ligand-free and salmeterol-bound receptor (Fig. 6d and Supplementary Fig. 11a), thus suggesting that TM6 did not move sufficiently far from TM5 in salmeterol-bound β2AR to decrease Atto655 quenching by Trp230. On the basis of the efficacy of salmeterol in G-protein activation (60% of isoproterenol; Supplementary Fig. 7c), we would expect a much larger change in Atto-β_2AR fluorescence in response to salmeterol if salmeterol and isoproterenol were to stabilize the same active state. The addition of Gs to salmeterol- and isoproterenol-bound Atto-β_2AR, as compared with ligand-free receptor, led to a 1.8- and 2.2-fold increase in fluorescence intensity, respectively (Fig. 6d, '+Gs' curves). This result is consistent with the G protein stabilizing an active conformation in a larger fraction of receptor. Control measurements on a construct without the engineered L230W mutation showed little intensity change after addition of agonists alone or together with Gs (Supplementary Fig. 11b). In line with the difference in TM6 outward motion between the Nb80- and Nb71-bound structures, the Atto response in the presence of Nb80 was much larger than that in the presence of Nb71, for both epinephrine and salmeterol (Supplementary Fig. 11c). This result was similar to our observations in the presence of Gs (Fig. 6b,d): when both ligand and Gs or nanobody were present, the TM6 receptor conformation was mainly stabilized by the intracellular binding protein and not the ligand. However, both of our fluorescence-based approaches in the absence of nanobody clearly suggested a difference in TM6 conformation between epinephrine- and salmeterol-bound receptors.

Discussion

β_2ARs expressed in airway smooth muscle and epithelial cells mediate bronchodilation and fluid clearance, respectively, and are thus well-established targets for the treatment of asthma and COPD[50]. The unusual pharmacological characteristics of salmeterol, including the extremely high selectivity for β_2AR and the long duration of action, which can be attributed to its long aryloxyalkyl tail, make salmeterol among the most commonly prescribed LABAs for treating asthma and COPD. Our structure reveals an additional site in the extracellular vestibule of β_2AR, the exosite, for the binding of the aryloxyalkyl tail, thus providing a structural basis for the prominent pharmacological action of salmeterol. It also resolves a long-standing debate regarding the location of the exosite.

Our results also provide structural insights into the partial agonism and the biased signaling properties of salmeterol, which are attributed to its saligenin ethanolamine group bound in the orthosteric binding pocket. Although the interactions with the receptor in the orthosteric binding pocket are very similar for the full agonist epinephrine and the partial agonist salmeterol, we observed subtle differences in hydrogen-bonding interactions. Most notable was the absence of interactions between salmeterol and Asn293$^{6.55}$, as further supported by MD simulations. The *meta*-hydroxyl of epinephrine forms a hydrogen bond with Asn293$^{6.55}$, which also forms a hydrogen bond with Ser204$^{5.43}$. Our mutagenesis studies suggest that this hydrogen-bond network may be important for stabilizing TM6 in a conformation necessary for efficient G-protein coupling as well as GRK phosphorylation and/or arrestin coupling. Therefore, the less extensive polar interactions between salmeterol and Asn293$^{6.55}$ may contribute to the weaker efficacy of salmeterol in activating Gs and the near absence of β-arrestin recruitment, possibly because of inefficient coupling as a result of decreased GRK phosphorylation[19].

The structure of salmeterol-bound β_2AR, compared with epinephrine-bound β_2AR, revealed a smaller outward movement of TM6. Although this conformation implies a 'partially active' conformation of the receptor, it is probably imposed by the nanobody Nb71 rather than by the partial agonist salmeterol. Previous studies have suggested relatively weak allosteric coupling between the orthosteric site and the cytoplasmic site[31]. Thus, capturing the ligand-specific conformation of β_2AR by protein crystallography is difficult. We used spectroscopic approaches with two different reporter systems to interrogate the conformational changes of β_2AR associated with salmeterol, and showed that TM6 indeed did not achieve the same extent of outward motion as that achieved by the full agonist epinephrine. This finding correlates with previous single-molecule investigations of TM6 motion in the β_2AR[33] and provides a structural basis for salmeterol's weaker Gs efficacy and possibly ligand bias. Whether this mechanism applies to other GPCRs requires further investigation.

Online content

Any methods, additional references, Nature Research reporting summaries, source data, statements of data availability and associated accession codes are available at https://doi.org/10.1038/s41589-018-0145-x.

Received: 9 May 2018; Accepted: 6 September 2018;
Published online: 16 October 2018

References

1. Kenakin, T. Drug efficacy at G protein–coupled receptors. *Annu. Rev. Pharmacol. Toxicol.* **42**, 349–379 (2002).
2. Zhu, B. T. Rational design of receptor partial agonists and possible mechanisms of receptor partial activation: a theory. *J. Theor. Biol.* **181**, 273–291 (1996).
3. Cazzola, M. & Donner, C. F. Long-acting β2 agonists in the management of stable chronic obstructive pulmonary disease. *Drugs* **60**, 307–320 (2000).
4. Baker, J. G., Proudman, R. G. & Hill, S. J. Salmeterol's extreme β2 selectivity is due to residues in both extracellular loops and transmembrane domains. *Mol. Pharmacol.* **87**, 103–120 (2015).
5. Ferguson, G. T., Funck-Brentano, C., Fischer, T., Darken, P. & Reisner, C. Cardiovascular safety of salmeterol in COPD. *Chest* **123**, 1817–1824 (2003).
6. Twentyman, O. P., Finnerty, J. P., Harris, A., Palmer, J. & Holgate, S. T. Protection against allergen-induced asthma by salmeterol. *Lancet* **336**, 1338–1342 (1990).

7. Ball, D. I. et al. Salmeterol, a novel, long-acting β2-adrenoceptor agonist: characterization of pharmacological activity in vitro and in vivo. *Br. J. Pharmacol.* **104**, 665–671 (1991).
8. Johnson, M. et al. The pharmacology of salmeterol. *Life Sci.* **52**, 2131–2143 (1993).
9. Calverley, P. M. et al. Salmeterol and fluticasone propionate and survival in chronic obstructive pulmonary disease. *N. Engl. J. Med.* **356**, 775–789 (2007).
10. Wijesinghe, M., Perrin, K., Harwood, M., Weatherall, M. & Beasley, R. The risk of asthma mortality with inhaled long acting β-agonists. *Postgrad. Med. J.* **84**, 467–472 (2008).
11. Weatherall, M., Wijesinghe, M., Perrin, K., Harwood, M. & Beasley, R. Meta-analysis of the risk of mortality with salmeterol and the effect of concomitant inhaled corticosteroid therapy. *Thorax* **65**, 39–43 (2010).
12. Coleman, R. A., Johnson, M., Nials, A. T. & Vardey, C. J. Exosites: their current status, and their relevance to the duration of action of long-acting beta 2-adrenoceptor agonists. *Trends Pharmacol. Sci.* **17**, 324–330 (1996).
13. Clark, R. B., Allal, C., Friedman, J., Johnson, M. & Barber, R. Stable activation and desensitization of beta 2-adrenergic receptor stimulation of adenylyl cyclase by salmeterol: evidence for quasi-irreversible binding to an exosite. *Mol. Pharmacol.* **49**, 182–189 (1996).
14. Green, S. A., Spasoff, A. P., Coleman, R. A., Johnson, M. & Liggett, S. B. Sustained activation of a G protein-coupled receptor via "anchored" agonist binding: molecular localization of the salmeterol exosite within the 2-adrenergic receptor. *J. Biol. Chem.* **271**, 24029–24035 (1996).
15. Isogaya, M. et al. Identification of a key amino acid of the β2-adrenergic receptor for high affinity binding of salmeterol. *Mol. Pharmacol.* **54**, 616–622 (1998).
16. Rong, Y. et al. Probing the salmeterol binding site on the β2-adrenergic receptor using a novel photoaffinity ligand, [^{125}I]iodoazidosalmeterol. *Biochemistry* **38**, 11278–11286 (1999).
17. Gimenez, L. E., Baameur, F., Vayttaden, S. J. & Clark, R. B. Salmeterol efficacy and bias in the activation and kinase-mediated desensitization of β 2-adrenergic receptors. *Mol. Pharmacol.* **87**, 954–964 (2015).
18. van der Westhuizen, E. T., Breton, B., Christopoulos, A. & Bouvier, M. Quantification of ligand bias for clinically relevant β2-adrenergic receptor ligands: implications for drug taxonomy. *Mol. Pharmacol.* **85**, 492–509 (2014).
19. Tran, T. M. et al. Characterization of agonist stimulation of cAMP-dependent protein kinase and G protein-coupled receptor kinase phosphorylation of the β2-adrenergic receptor using phosphoserine-specific antibodies. *Mol. Pharmacol.* **65**, 196–206 (2004).
20. Drake, M. T. et al. β-arrestin-biased agonism at the β2-adrenergic receptor. *J. Biol. Chem.* **283**, 5669–5676 (2008).
21. Carter, A. A. & Hill, S. J. Characterization of isoprenaline- and salmeterol-stimulated interactions between β2-adrenoceptors and β-arrestin 2 using β-galactosidase complementation in C2C12 cells. *J. Pharmacol. Exp. Ther.* **315**, 839–848 (2005).
22. Moore, R. H. et al. Salmeterol stimulation dissociates β2-adrenergic receptor phosphorylation and internalization. *Am. J. Respir. Cell Mol. Biol.* **36**, 254–261 (2007).
23. Walker, J. K. & DeFea, K. A. Role for β-arrestin in mediating paradoxical β2AR and PAR2 signaling in asthma. *Curr. Opin. Pharmacol.* **16**, 142–147 (2014).
24. Billington, C. K., Penn, R. B. & Hall, I. P. β_2 agonists. *Handb. Exp. Pharmacol.* **237**, 23–40 (2017).
25. Rasmussen, S. G. et al. Structure of a nanobody-stabilized active state of the β_2 adrenoceptor. *Nature* **469**, 175–180 (2011).
26. Rasmussen, S. G. et al. Crystal structure of the β_2 adrenergic receptor–Gs protein complex. *Nature* **477**, 549–555 (2011).
27. Rosenbaum, D. M. et al. Structure and function of an irreversible agonist–β_2 adrenoceptor complex. *Nature* **469**, 236–240 (2011).
28. Warne, T. et al. The structural basis for agonist and partial agonist action on a β_1-adrenergic receptor. *Nature* **469**, 241–244 (2011).
29. Ring, A. M. et al. Adrenaline-activated structure of β_2-adrenoceptor stabilized by an engineered nanobody. *Nature* **502**, 575–579 (2013).
30. Nygaard, R. et al. The dynamic process of β_2-adrenergic receptor activation. *Cell* **152**, 532–542 (2013).
31. Manglik, A. et al. Structural insights into the dynamic process of β 2-adrenergic receptor signaling. *Cell* **161**, 1101–1111 (2015).
32. Sounier, R. et al. Propagation of conformational changes during μ-opioid receptor activation. *Nature* **524**, 375–378 (2015).
33. Gregorio, G. G. et al. Single-molecule analysis of ligand efficacy in β $_2$AR–G-protein activation. *Nature* **547**, 68–73 (2017).
34. Staus, D. P. et al. Regulation of β2-adrenergic receptor function by conformationally selective single-domain intrabodies. *Mol. Pharmacol.* **85**, 472–481 (2014).
35. Zou, Y., Weis, W. I. Kobilka, B. K. & Seifert, R. N-terminal T4 lysozyme fusion facilitates crystallization of a G protein coupled receptor. *PLoS One* **7**, e46039 (2012).
36. Caffrey, M. Crystallizing membrane proteins for structure determination: use of lipidic mesophases. *Annu. Rev. Biophys.* **38**, 29–51 (2009).
37. Baker, J. G. The selectivity of β-adrenoceptor agonists at human β1-, β2- and β3-adrenoceptors. *Br. J. Pharmacol.* **160**, 1048–1061 (2010).
38. Kruse, A. C. et al. Activation and allosteric modulation of a muscarinic acetylcholine receptor. *Nature* **504**, 101–106 (2013).
39. Fronik, P., Gaiser, B. I. & Sejer Pedersen, D. Bitopic ligands and metastable binding sites: opportunities for G protein-coupled receptor (GPCR) medicinal chemistry. *J. Med. Chem.* **60**, 4126–4134 (2017).
40. Wieland, K., Zuurmond, H. M., Krasel, C., Ijzerman, A. P. & Lohse, M. J. Involvement of Asn-293 in stereospecific agonist recognition and in activation of the β2-adrenergic receptor. *Proc. Natl. Acad. Sci. USA* **93**, 9276–9281 (1996).
41. Liapakis, G., Chan, W. C., Papadokostaki, M. & Javitch, J. A. Synergistic contributions of the functional groups of epinephrine to its affinity and efficacy at the β2 adrenergic receptor. *Mol. Pharmacol.* **65**, 1181–1190 (2004).
42. Thomsen, A. R. B. et al. GPCR-G protein-β-arrestin super-complex mediates sustained G protein signaling. *Cell* **166**, 907–919 (2016).
43. Namkung, Y. et al. Monitoring G protein-coupled receptor and β-arrestin trafficking in live cells using enhanced bystander BRET. *Nat. Commun.* **7**, 12178 (2016).
44. Picard, L.-P., Schönegge, A. M., Lohse, M. J. & Bouvier, M. Bioluminescence resonance energy transfer-based biosensors allow monitoring of ligand- and transducer-mediated GPCR conformational changes. *Commun. Biol.* **1**, 106 (2018).
45. Yao, X. J. et al. The effect of ligand efficacy on the formation and stability of a GPCR-G protein complex. *Proc. Natl. Acad. Sci. USA* **106**, 9501–9506 (2009).
46. Dawaliby, R. et al. Allosteric regulation of G protein–coupled receptor activity by phospholipids. *Nat. Chem. Biol.* **12**, 35–39 (2016).
47. Schafer, C. T., Fay, J. F., Janz, J. M. & Farrens, D. L. Decay of an active GPCR: conformational dynamics govern agonist rebinding and persistence of an active, yet empty, receptor state. *Proc. Natl. Acad. Sci. USA* **113**, 11961–11966 (2016).
48. Fay, J. F. & Farrens, D. L. Purification of functional CB_1 and analysis by site-directed fluorescence labeling methods. *Methods Enzymol.* **593**, 343–370 (2017).
49. Doose, S., Neuweiler, H. & Sauer, M. A close look at fluorescence quenching of organic dyes by tryptophan. *Chemphyschem* **6**, 2277–2285 (2005).
50. Cazzola, M., Calzetta, L. & Matera, M. G. β_2-adrenoceptor agonists: current and future direction. *Br. J. Pharmacol.* **163**, 4–17 (2011).

Acknowledgements

This work was supported by National Institutes of Health grant R01NS028471 (B.K.K.), Canadian Institute for Health Research foundation grant FDN-148431 (M.B.), an American Heart Association Postdoctoral fellowship (17POST33410958; M.M.) and Predoctoral Fellowship (13PRE17110027; J.P.M.), a studentship from the FRQ-S (L.-P.P.), the NIH Pharmacological Sciences Training Program (T32GM007767; J.P.M.) and the National Institutes of Health MIRA 1R35GM128641-01 (C.Z.). B.K.K. is supported by the Chan Zuckerberg Biohub. M.B. is supported as a Canada Research Chair in Signal Transduction and Molecular Pharmacology. The authors thank J. Gullingsrud for assistance with MD software.

Author contributions

C.Z. and Y.Z. expressed and purified the receptor and nanobody for crystallography studies, collected X-ray diffraction data and solved the crystal structure. M.M. developed the Atto655 reporter system; purified and labeled receptors used in fluorescence studies; collected spectroscopic data; and performed radioactive ligand binding assays. L.-P.P. generated mutants of N293 and S204. E.v.d.W. and L.-P.P. performed Gs-activation and β-arrestin2-recruitment BRET assays under supervision from M.B. J.P.M. performed Octet RED experiments under supervision from R.K.S. J.P.G.L.M.R. performed modeling and sampling of the Atto655 dye on the receptor structures. T.J.M. and R.O.D. performed and analyzed MD-simulation studies. R.O.D. and D.E.S. oversaw MD simulations and analysis. E.P. generated the nanobody library and performed the initial selections. J.S. supervised nanobody production. W.I.W. supervised and assisted with the structure refinement. M.M., C.Z. and B.K.K. interpreted data, made figures and wrote the manuscript. B.K.K. provided overall project supervision.

Competing interests

The BRET-based biosensors used in the present study are licensed to Domain Therapeutics but are freely available from M.B. for noncommercial academic use. M.B. is the chair of the Scientific Advisory Board of Domain Therapeutics. B.K.K. is a cofounder of and consultant for ConfometRx.

Additional information

Supplementary information is available for this paper at https://doi.org/10.1038/s41589-018-0145-x.

Reprints and permissions information is available at www.nature.com/reprints.

Correspondence and requests for materials should be addressed to C.Z. or B.K.K.

Publisher's note: Springer Nature remains neutral with regard to jurisdictional claims in published maps and institutional affiliations.

Methods

Receptor constructs. All constructs had an N-terminal FLAG tag. The T4L-β_2AR-ΔICL3 construct consisted of an N-terminal T4 lysozyme fusion to β_2AR(29–365)-ΔICL3, i.e., Δ(235–263) with mutations M96T, M98T and N187E. The β_2AR-PN1 construct consisted of the β_2(1–24)-TEV-β_2(25–365)-3C-β_2(366–413) construct, with TEV and 3C indicating tobacco etch virus (TEV) protease and 3C protease cut sites, respectively. Additionally, mutations M96T, M98T, C378A, N187E and C406A were introduced, as previously described[46]. The β_2ARΔ6 L230W L266C construct consisted of a full-length wild-type receptor with a minimal cysteine background[33] (C77V, C265A, C327S, C341L, C378A and C406A) as well as mutations L230W and L266C and a C-terminal hexahistidine tag.

Expression, purification and labeling of β_2AR constructs. Receptor constructs were expressed in *Sf*9 insect-cell cultures infected with recombinant baculovirus (BestBac, Expression Systems) and solubilized in *n*-dodecyl-β-D-maltoside (DDM) according to methods described previously[46]. The solubilized receptor was purified through M1 FLAG chromatography followed by alprenolol–Sepharose chromatography to remove nonfunctional receptor[46]. A second M1 FLAG chromatography step was performed such that the receptor-bound alprenolol could be removed for ligand-free protein or exchanged for salmeterol.

For the T4L-β_2AR-ΔICL3, after the protein was eluted from the M1 resin, the FLAG epitope tag of T4L-β_2AR-Δ-ICL3 was removed by treatment with TEV protease (Invitrogen) for 3 h at room temperature or overnight at 4 °C. When necessary, a 50-kDa MWCO Vivaspin concentrator (GE Healthcare) was used to concentrate the receptor. The β_2AR constructs used for fluorescence studies were concentrated and flash-frozen in the presence of 20% glycerol at a final concentration of 200 μM. Aliquots were then stored at −80 °C until use.

Full-length PN1-β_2AR was labeled with monobromobimane as previously described[51]. Briefly, FLAG pure receptor (~2 μM) was incubated overnight on ice with 100 μM TCEP and 20 μM monobromobimane (Thermo Fisher Scientific). Subsequently, 5 mM cysteine was added to quench the labeling reaction, and alprenolol–Sepharose chromatography was performed as described above. A similar procedure was followed for labeling β_2ARΔ6 L230W L266C with Atto655-iodoacetamide (Atto-TEC).

G-protein expression and purification. Wild-type Gs heterotrimer was expressed and purified as previously described[33]. After purification, the protein was dialyzed into 20 mM HEPES, pH 7.5, 100 mM NaCl, 0.02% DDM, 100 μM TCEP and 20 μM GDP, concentrated, and flash-frozen in the presence of 20% glycerol at a final concentration of 200 μM. Aliquots were then stored at −80 °C until use.

Preparation of Nb71 and Nb80. The recombinant Nb71 was generated in the same way as Nb80 (ref. [25]). These two nanobodies were screened from an identical library of single-chain nanobody clones after immunization of a llama with purified agonist-bound β_2AR reconstituted at high density into phospholipid vesicles. Nb71 was expressed in *Escherichia coli* and purified by nickel-affinity chromatography in the same manner as Nb80 (ref. [25]). The protein was then further purified by cation exchange with a Mono-S column (GE Healthcare); the protein was loaded in 20 mM NaCl and 20 mM MES, pH 6.0, and eluted with a linear gradient from 50 to 500 mM NaCl. To minimize severe precipitation of Nb71 over time, the purified protein was stored at a concentration below 5 mg/mL in 20 mM HEPES and 1 M NaCl.

Crystallization. Salmeterol-bound receptor (~40 mg/mL) was incubated with a 5.5-fold molar excess of Nb71 (~50 mg/mL) for 1 h on ice. Size-exclusion chromatography was then performed to remove free Nb71. The purified complex was concentrated to ~60 mg/mL for crystallization with the lipid cubic phase method as previously described[36]. The protein complex was reconstituted in mono-olein containing 10% cholesterol at a 1:1.5 protein/lipid ratio (wt/wt). Drops of reconstituted protein–lipid mixture (30 nL) were deposited in each well of a 96-well glass sandwich plate (Molecular Dimensions). The drop was then overlaid with 650 nL of precipitant, and the wells were sealed with a glass coverslip. Diffraction-quality crystals were grown at 20 °C in 31–34% PEG 400, 100 mM HEPES, pH 7.5, and 1% 1,2,3-heptanetriol after 3 d of incubation at 20 °C.

Data collection, structure determination and analysis. Crystals were harvested and frozen in liquid nitrogen directly without use of additional cryoprotectant. Diffraction data from 24 different crystals were measured with the GM/CA-CAT microfocus beam at 23-ID-D (Advanced Photon Source, Argonne National Labs). The data were processed with HKL2000, and the structure was solved by molecular replacement with Phaser. Further model rebuilding was performed with Coot, and the structure was refined with Phenix. The validation of the final structural model was performed with MolProbity. The overall MolProbity score was 1.35. In Ramachandran analysis, 96.8% of atoms were in favored regions, and 3.2% of atoms were in allowed regions. Data processing and refinement statistics are shown in Supplementary Table 2.

The structure of the inactive β_2AR (PDB 2RH1); β_2AR in complex with Nb80 (PDB 3P0G); β2AR in complex with Gs (PDB 3SN6); and chain A of sabultamol bound to β_1AR (PDB 2Y04) were used for structural alignments in PyMOL, on the basis of Cα only. The secondary structure of β_2AR ICL2 was assigned with PyMOL and DSSP.

Reconstitution of β_2AR in HDL particles for Octet RED measurements. The β_2AR was reconstituted in high-density lipoprotein (HDL) particles through established methods[46]. The scaffold protein ApoA-I used for reconstitution was purified as previously described[46]. Purified ApoA-I was biotinylated for 30 min at room temperature with NHS–PEG4–biotin (Thermo) at a 1:1 molar ratio in a buffer composed of 20 mM HEPES, pH 8.0, 100 mM NaCl, 1 mM EDTA and 5 mM sodium cholate. After the labeling reaction, unreacted biotin was quenched by the addition of Tris-HCl, pH 8.0, to a final concentration of 20 mM. Biotinylated protein was separated from free biotin by size-exclusion chromatography on a Superdex 75 HR 10/30 column. FLAG-tagged β_2AR was incorporated into HDL particles with biotinylated ApoA-I, and receptor-containing HDL particles were isolated through M1 anti-FLAG immunoaffinity chromatography.

Nanobody binding to β_2AR in biotinylated HDL particles was monitored with an Octet RED biolayer interferometry system (Pall FortéBio) with streptavidin-coated biosensors (Pall FortéBio). Sensors were hydrated for at least 10 min at room temperature in assay buffer (20 mM Tris-HCl, pH 7.4, 136 mM NaCl, 2.7 mM KCl, 1 mM EDTA, 0.02% (wt/vol) ascorbic acid and 0.05% (wt/vol) BSA), then incubated with biotinylated β_2AR–HDL (~100 nM) for 10 min at room temperature before the sensors were loaded onto the Octet RED instrument. All steps on the Octet RED instrument were performed at 25 °C with the assay plate shaking at 1,000 r.p.m. After an initial baseline reading, sensors were dipped into wells containing assay buffer with a saturating concentration of agonist (100 μM epinephrine, 0.1 μM BI-167107 or 1 μM salmeterol) and incubated for 20 min to equilibrate β_2AR with the agonist. The sensors were transferred to wells containing assay buffer plus agonist and nanobody (1, 3.2, 10, 32, 100 or 320 nM) for 5 min to monitor nanobody association. Nanobody dissociation was then monitored by transferring the sensors to wells containing assay buffer plus agonist for 30 min. Nonspecific nanobody binding at each concentration was measured in a parallel experiment in which sensors were loaded with empty HDL. Buffer-only controls were also included in each experiment to correct for baseline drift. Data were first analyzed in Octet Data Analysis 7.0 software (Pall FortéBio) to remove baseline and nonspecific binding, and the processed data were exported to Prism 6 (GraphPad) for curve fitting. All association and dissociation curves were fit with single-phase exponential association or decay.

BRET measurements for Gs activation, β-arrestin recruitment and β_2AR conformational changes in live cells. HEK293T cells used for the BRET assays were grown in Dulbecco's modified Eagle's medium supplemented with 10% newborn calf serum, at 37 °C with 5% CO_2. Cells were detached with trypsin–EDTA and transfected with 2.5 μg of total DNA per 10^6 cells, with linear polyethyleneimine (Polysciences) as a transfecting agent, at a ratio of 3:1 polyethyleneimine/DNA. Gs activation was evaluated with Gs-117-RLucII/Gβ 1/Gγ1-GFP10 (ref. [42]), and β-arrestin recruitment was evaluated with CAAX-rGFP/β-arr2-RLucII[43] sensors, in the presence of wild-type 3HA-β_2AR or mutant receptors. The conformational changes were detected with the NY-β_2AR sensor[44]. Directly after transfection, cells were plated in white 96-well plates (Greiner) at a density of 50,000 cells/well and incubated for 48 h. The plates were then washed with PBS, and assay buffer (Hank's balanced salt solution) was added. Cells were stimulated with the ligands during 5 or 15 min for evaluation of Gs activation or β-arrestin recruitment and conformational changes, respectively. Coelenterazine 400a (2.5 μM) was added 5 min before the reads. BRET was monitored with a TriStar LB942 microplate reader (Berthold) equipped with a 410/80-nm donor filter and a 515/40-nm acceptor filter (for Gs activation and β-arrestin recruitment) or a 485/20-nm donor filter and a 530/25-nm acceptor filter (for receptor conformational changes). The BRET ratio was calculated by dividing the acceptor emission by the donor emission. The data were analyzed in Prism (GraphPad) by using 'dose-response- stimulation log(agonist) vs normalized response- variable slope' with the constraint of sharing the Hill slope across all datasets.

Molecular dynamics simulations. We simulated the β_2AR bound to the partial agonist salmeterol as well as the full agonist epinephrine. We initiated these simulations from crystal structures of the receptor bound to each of these ligands. Each of the crystal structures that we used includes a nanobody that binds to the intracellular side of the receptor and stabilizes an active or intermediate receptor state: Nb71 for salmeterol and Nb6B9 for epinephrine[29].

We performed three simulations of β_2AR–salmeterol–Nb71 and three simulations of β_2AR–epinephrine–Nb6B9. Each of the crystallized constructs was a β_2AR-T4L fusion protein, with T4L replacing the receptor's N terminus. T4L was omitted from all simulations, whereas all other resolved residues were included. Most of ICL3 was absent in all simulations, because it was deleted from the crystallized construct in β_2AR–salmeterol–Nb71 and β_2AR–epinephrine–Nb6B9. Because the simulations were performed before the published coordinates had been finalized, they were initiated by using coordinates that differed very slightly from the published ones (r.m.s. deviation below 0.3 Å, computed over all resolved receptor Cα atoms); these differences were much smaller than the typical motions of the atoms in simulation. In all simulations, a palmitoyl group that was not

resolved but was presumed to be present in the crystallized constructs was added to Cys341 with Maestro (Schrödinger).

The β_2AR was embedded in a hydrated lipid bilayer in all simulations; all atoms (including those in lipids and water) were represented explicitly. Hydrogen atoms were added to the crystal structures with Maestro, as described previously, and receptor chain termini were capped with neutral groups (acetyl and methylamide). Titratable residues other than Glu122$^{3.41}$ were left in their dominant protonation states at pH 7.0. Glu122$^{3.41}$, which faces the lipid bilayer, was neutral (protonated) in all simulations.

The prepared protein structures were inserted into an equilibrated bilayer solvated with 0.15 M NaCl, through a previously described protocol[52]. The bilayer consisted of palmitoyl-oleoyl-phosphatidylcholine, with 24% palmitoyl-oleoyl-phosphatidylserine in the inner-membrane leaflet. The simulated systems initially measured approximately $71 \times 71 \times 115$ Å^3 and contained approximately 140 lipid molecules, 12,000 water molecules, 32 chloride ions and 40 sodium ions.

We also performed three simulations of β_2AR–salmeterol with the nanobodies removed (but otherwise starting from the same structures as above). The simulation setup was as described above, except that the removal of the nanobody allowed for the simulated volume to be somewhat smaller. These simulations initially measured approximately $69 \times 69 \times 85$ Å^3 and contained approximately 120 lipid molecules, 7,200 water molecules, 19 chloride ions and 30 sodium ions.

We used the CHARMM-h force field for proteins. We used the CHARMM36 lipid force field along with standard CHARMM salt-ion parameters and the CHARMM TIP3P model for water. The parameters for palmitoyl-cysteine were as described previously[27,52], and the parameters for epinephrine were obtained by adaptation of previously published parameters for isoproterenol[53]. The parameters for salmeterol were obtained from the ParamChem server. Full parameter sets are available upon request.

Each simulation consisted of a 50-ns equilibration run followed by a longer production run. Systems were equilibrated in the NPT ensemble (310 K, 1 bar, Martyna–Tuckerman–Klein–Nosé–Hoover chain-coupling scheme using a multigrator, with initial velocities sampled from the Boltzmann distribution and with 5 kcal mol^{-1} Å^{-2} harmonic position restraints applied to the protein and ligand atoms, which were tapered off linearly over 50 ns. Production simulations used the same integrator, pressure and temperature, and were initiated from the final snapshot of the corresponding equilibration simulation. All simulations were performed on an Anton 1 computer[54].

All bond lengths to hydrogen atoms were constrained with M-SHAKE. An r-RESPA integrator was used with a time step of 2.5 fs, and long-range electrostatics were computed every 7.5 fs. Long-range electrostatics were computed in reciprocal space with the *u*-series method[55].

Simulation snapshots were saved every 180 ps. For the purposes of evaluating the fraction of time, a hydrogen bond was formed in simulation; such a bond was considered to be formed in snapshots in which the relevant nonhydrogen atoms were within 3.0 Å of one another. Because the bound ligands shifted in pose during the later parts of certain simulations (possibly as a result of motion of the nanobodies, which are not held in place by crystallographic contacts), we used the first microsecond of each simulation for these analyses. Each error bar was calculated as s.e.m. across three simulations.

Dye modeling. The structure of the iodoacetamide derivative of the Atto655 dye (Atto-TEC) was obtained from PubChem (CID 16218785) and optimized with Avogadro and the GAFF force field. The structures of β_2AR in the active (PDB 3SN6) and inactive conformations (PDB 2RH1) were retrieved from the RCSB Protein Data Bank and mutated (L230W and L266C) with PyMOL. The parameters for the dye molecule attached to a cysteine residue were obtained with PRODRG and manually edited to enforce the planarity of the ring system of the dye. Crystallography and NMR System (CNS) software, version 1.3 (ref. [56]), was used to attach the dye to L266C and simulate its positions through rigid-body docking and multitrial simulated annealing, respectively, as previously performed by Brunger and co-workers[57]. The entire receptor structure was kept rigid except for the side-chain atoms of L230W and L266C. Distances between the centers of mass of the tryptophan side-chain atoms and the center of mass of the ring system of the dye were calculated for each generated model (300 for each conformation of β_2AR).

Fluorescence measurements on purified receptor in detergent solution. Bimane-labeled and Atto-labeled receptors were used at respective concentrations of 0.2 µM and 0.1 µM in buffer containing 20 mM HEPES, pH 7.4, 100 mM NaCl, 0.02% (wt/vol) DDM and 0.002% (wt/vol) cholesterol hemisuccinate. Salmeterol and epinephrine stocks were prepared as 50 mM and 100 mM solutions in DMSO and added at the indicated final concentrations. Ligand concentrations were chosen to achieve saturation of detergent-solubilized receptor. To avoid any nonspecific vehicle effects, care was taken to obtain the same final concentration of DMSO in all samples. Where indicated, Gs was added to a final concentration of 2 µM. To allow for efficient ligand binding and full equilibration, samples were incubated at the final concentrations used for 1 h in the dark before measurements. Fluorescence data were collected in a quartz cuvette with 500 µL of sample in FluorEssence v3.8 software on a Fluorolog instrument (Horiba) in photon-counting mode. Bimane fluorescence was measured by excitation at 370 nm with excitation and emission bandwidth passes of 4 nm, and emission spectra were recorded from 410 to 510 nm in 1-nm increments and 1-s integration time. Atto fluorescence was measured by excitation at 650 nm with excitation and emission bandwidth passes of 5 nm, and emission spectra were recorded from 660 to 730 nm in 1-nm increments and 1-s integration time. Measurements were performed in triplicate.

Radioligand binding assays. Binding curves were obtained by incubation of DDM-purified wild-type and bimane- and Atto655-labeled receptors in the presence of M1 FLAG–Sepharose and 2 mM Ca^{2+}, under shaking at room temperature for 1.5 h. The antagonist [^{3}H]dihydroalprenolol (PerkinElmer) was used to obtain saturation binding curves. Competition binding measurements for salmeterol and epinephrine were performed in a similar way, with [^{3}H] dihydroalprenolol at a concentration slightly above the K_d, as determined by saturation binding. Nonspecific binding was accounted for by measurements in the presence of 10 µM cold alprenolol. Beads were harvested with a 48-well Brandell harvester and counted in a LS6000TA scintillator (Beckman) with Cytoscint (MP Biomedical).

Statistical analysis. The statistical significance of hydrogen-bond duration from MD trajectories (Fig. 5a) was assessed with one-sided Welch's unequal variance *t* tests. The statistical significance of the binding affinities (Supplementary Table 1) was assessed with ordinary one-way ANOVA (Tukey) test at a multiplicity-adjusted *P*-value cutoff of 0.05. The statistical significance of the fitted mean log(K_i) values (Supplementary Fig. 1) was assessed with a one-way ANOVA Tukey test at a *P*-value cutoff of 0.05 (adjusted for multiple comparisons).

Reporting Summary. Further information on research design is available in the Nature Research Reporting Summary linked to this article.

Data availability

Atomic coordinates and structure factors for the crystal structure have been deposited in the Protein Data Bank under accession code PDB 6CSY. Other data and results are available upon request.

References

51. Rosenbaum, D. M. et al. GPCR engineering yields high-resolution structural insights into β2-adrenergic receptor function. *Science* **318**, 1266–1273 (2007).
52. Dror, R. O. et al. Identification of two distinct inactive conformations of the β2-adrenergic receptor reconciles structural and biochemical observations. *Proc. Natl. Acad. Sci. USA* **106**, 4689–4694 (2009).
53. Dror, R. O. et al. Pathway and mechanism of drug binding to G-protein-coupled receptors. *Proc. Natl. Acad. Sci. USA* **108**, 13118–13123 (2011).
54. Shaw, D. E. et al. Millisecond-scale molecular dynamics simulations on Anton. *Proc. Conf. High Perform. Comput. Netw. Storage Anal.* (pp. 1–11. ACM, Portland, Oregon, USA, 2009).
55. Shaw, D. E. et al. Anton 2: raising the bar for performance and programmability in a special-purpose molecular dynamics supercomputer. *Sc14: Int. Conf. High Perform. Comput., Netw. Storage Anal.* (pp. 41–53. IEEE, Hoboken, New Jersey, USA, 2014).
56. Brunger, A. T. Version 1.2 of the Crystallography and NMR system. *Nat. Protoc.* **2**, 2728–2733 (2007).
57. Choi, U. B. et al. Single-molecule FRET-derived model of the synaptotagmin 1-SNARE fusion complex. *Nat. Struct. Mol. Biol.* **17**, 318–324 (2010).

nature research

Corresponding author(s): Cheng Zhang, Brian Kobilka

Reporting Summary

Nature Research wishes to improve the reproducibility of the work that we publish. This form provides structure for consistency and transparency in reporting. For further information on Nature Research policies, see Authors & Referees and the Editorial Policy Checklist.

Statistical parameters

When statistical analyses are reported, confirm that the following items are present in the relevant location (e.g. figure legend, table legend, main text, or Methods section).

n/a	Confirmed	
☐	☒	The exact sample size (*n*) for each experimental group/condition, given as a discrete number and unit of measurement
☐	☒	An indication of whether measurements were taken from distinct samples or whether the same sample was measured repeatedly
☐	☒	The statistical test(s) used AND whether they are one- or two-sided *Only common tests should be described solely by name; describe more complex techniques in the Methods section.*
☒	☐	A description of all covariates tested
☒	☐	A description of any assumptions or corrections, such as tests of normality and adjustment for multiple comparisons
☐	☒	A full description of the statistics including central tendency (e.g. means) or other basic estimates (e.g. regression coefficient) AND variation (e.g. standard deviation) or associated estimates of uncertainty (e.g. confidence intervals)
☐	☒	For null hypothesis testing, the test statistic (e.g. *F*, *t*, *r*) with confidence intervals, effect sizes, degrees of freedom and *P* value noted *Give P values as exact values whenever suitable.*
☒	☐	For Bayesian analysis, information on the choice of priors and Markov chain Monte Carlo settings
☒	☐	For hierarchical and complex designs, identification of the appropriate level for tests and full reporting of outcomes
☒	☐	Estimates of effect sizes (e.g. Cohen's *d*, Pearson's *r*), indicating how they were calculated
☐	☒	Clearly defined error bars *State explicitly what error bars represent (e.g. SD, SE, CI)*

Our web collection on statistics for biologists may be useful.

Software and code

Policy information about availability of computer code

Data collection	Octet Red data were collected using OctetRED biolayer interferometry system (Pall FortéBio). Fluorescence data were collected using FluorEssence v3.8 (Horiba). Molecular dynamics simulations were performed on Anton (Assoc Computing Machinery, New York).
Data analysis	Octet data were processed using Octet Data Analysis 7.0 software (Pall FortéBio) to remove baseline and nonspecific binding and further analyzed in Prism 6 (GraphPad) for curve fitting. Crystallography data were processed with HKL2000 and the structure solved by molecular replacement using Phaser. Further model rebuilding was performed by using Coot and the structure was refined with Phenix. The validation of the final structural model was performed using Molprobity. BRET data were analyzed in Prism 7 (GraphPad). For simulations, a palmitoyl group not resolved but presumed to be present in the crystallized constructs was added to Cys341 using Maestro (Schrödinger LLC, New York, NY). The structure of the iodoacetamide derivative of the Atto655 dye was optimized using Avogadro and the GAFF force field. Parameters for the dye molecule attached to a cysteine residue were obtained using PRODRG. The Crystallography and NMR System (CNS) software, version 1.3, was used to attach the dye to L266C and simulate its positions. Radioligand binding data were analyzed in Prism 7 (GraphPad) using "One site -- Total and nonspecific binding" for saturation binding and "Nonlinear Regression - One site - Fit Ki" fitting for competition binding. Figures for structures were made in PyMOL v1.8.4.1 (Schrödinger). The 2-D representation ligand plot figure was generated using LigPlot+. Fluorescence data were analyzed in Prism 7 (GraphPad).

For manuscripts utilizing custom algorithms or software that are central to the research but not yet described in published literature, software must be made available to editors/reviewers upon request. We strongly encourage code deposition in a community repository (e.g. GitHub). See the Nature Research guidelines for submitting code & software for further information.

Data

Policy information about availability of data

All manuscripts must include a data availability statement. This statement should provide the following information, where applicable:

- Accession codes, unique identifiers, or web links for publicly available datasets
- A list of figures that have associated raw data
- A description of any restrictions on data availability

Atomic coordinates and the structure factors for the crystal structure have been deposited with the Protein Data Bank under accession code 6CSY. Other data and results are available upon request.

Field-specific reporting

Please select the best fit for your research. If you are not sure, read the appropriate sections before making your selection.

☒ Life sciences ☐ Behavioural & social sciences ☐ Ecological, evolutionary & environmental sciences

For a reference copy of the document with all sections, see nature.com/authors/policies/ReportingSummary-flat.pdf

Life sciences study design

All studies must disclose on these points even when the disclosure is negative.

Sample size	No animal studies were performed in this study. No statistical method was used to predetermine sample size. For all measurements, the experimental methods are conventional and widely used, and detailed and cited in the methods section. According to general convention for these methods, 3 to 5 replicate measurements are sufficient to obtain statistical significance (calculation of mean and standard deviation or standard error of the mean) to allow to draw scientific conclusions.
Data exclusions	No data were excluded from the analyses.
Replication	All attempts at replication were successful.
Randomization	No animal or behavioral studies were performed in this study. Data collection (computer simulation, X-ray diffraction, fluorescence, luminescence, interferometry and photon counting - liquid scintillation) was performed by setups that are independent from the experimenter when collected. Randomization was thus not necessary in our study and was not performed.
Blinding	Similar to what is mentioned above, blinding was not necessary for our study and was not performed.

Reporting for specific materials, systems and methods

Materials & experimental systems

n/a	Involved in the study
☐	☒ Unique biological materials
☐	☒ Antibodies
☐	☒ Eukaryotic cell lines
☒	☐ Palaeontology
☒	☐ Animals and other organisms
☒	☐ Human research participants

Methods

n/a	Involved in the study
☒	☐ ChIP-seq
☒	☐ Flow cytometry
☒	☐ MRI-based neuroimaging

Unique biological materials

Policy information about availability of materials

Obtaining unique materials	Nanobody 71, a camelid antibody can be obtained from Jan Steyaert, Structural Biology Brussels, Vrije Universiteit Brussel, Brussels, Belgium

Antibodies

Antibodies used	Nanobody 71 is a camelid antibody generated by the laboratory of Jan Steyaert with protein produced in the laboratory of Brian Kobilka
Validation	Nanobody 71 is validated by functional studies outlined in the manuscript and by a crystal structure showing the binding of Nanobody 71 to the beta-2 adrenergic receptor.

Eukaryotic cell lines

Policy information about cell lines

Cell line source(s)	The Sf9 insect cell line used was obtained from Expression Systems and is a clonal isolate derived from the parental Spodoptera frugiperda cell line IPLB-Sf-21-AE. The HEK293 cell line used in this study is the one in which BRET-based biosensors have been developed in Dr Michel Bouvier's laboratory.
Authentication	No authentication required.
Mycoplasma contamination	The HEK293 cells were regularly tested for mycoplasma contamination (PCR Mycoplasma Detection kit, abm, BC, Canada) and used only if contamination-free.
Commonly misidentified lines (See ICLAC register)	Cells are not listed in the database.